A method for tensile tests of biological tissues at the mesoscale

Thierry Savin, Amy E. Shyer, and L. Mahadevan

Related Articles

Suppression of scar formation in a murine burn wound model by the application of non-thermal plasma
Appl. Phys. Lett. 99, 203701 (2011)

Longitudinal variations in the Poisson's ratio of collagen fibrils
Appl. Phys. Lett. 98, 163707 (2011)

In vivo nanomechanical imaging of blood-vessel tissues directly in living mammals using atomic force microscopy
Appl. Phys. Lett. 95, 013704 (2009)

Detection and discrimination of optical absorption and shear stiffness at depth in tissue-mimicking phantoms by transient optoelastography
Appl. Phys. Lett. 94, 154103 (2009)

Effects of hydration on the mechanical response of individual collagen fibrils
Appl. Phys. Lett. 92, 233902 (2008)

Additional information on J. Appl. Phys.

Journal Homepage: http://jap.aip.org/

Journal Information: http://jap.aip.org/about/about_the_journal

Top downloads: http://jap.aip.org/features/most_downloaded

Information for Authors: http://jap.aip.org/authors

A method for tensile tests of biological tissues at the mesoscale

Thierry Savin,[1,a)] Amy E. Shyer,[2] and L. Mahadevan[1,3,b)]
[1]*School of Engineering and Applied Sciences, Harvard University, Cambridge, Massachusetts 02138, USA*
[2]*Department of Genetics, Harvard Medical School, Boston, Massachusetts 02115, USA*
[3]*Department of Physics, Harvard University, Cambridge, Massachusetts 02138, USA*

We describe a new technique for determining the tensile properties of biological tissues at the mesoscale. The procedure uses a calibrated magnetic interaction between a steel bead attached to the sample and a permanent magnet to apply a uniaxial tensile force, along with a simple video assay to monitor the sample extension and thus the strain. Our method fills a significant gap in the accessible range of both forces and strains and is useful for forces in the micro and milli-Newton range, and displacements in the range of hundreds of microns with strains of up to 200%. We give two examples of the mechanical characterization of tissues using our technique, employing it to characterize the elastic modulus of tubular and membraneous embryonic tissues from the chick. © 2012 American Institute of Physics. [http://dx.doi.org/10.1063/1.3699176]

I. INTRODUCTION

Tensile testing is an important method for the mechanical characterization of soft and hard matter.[1] Depending on the sample size and the magnitude of the response, different techniques are employed to measure the load-deformation response. For example, optical traps are used to stretch single molecules and cells,[2] with forces in the 10^{-12}-10^{-10} N range applied in order to measure displacements $\lesssim 10^{-6}$ m. On a larger scale, flexible rods (e.g., glass optical fibers) are used to measure the properties of early stage embryonic tissues,[3,4] with forces between 10^{-9} and 10^{-6} N and displacements $\lesssim 10^{-4}$ m. The gauging of forces $>10^{-2}$ N on $\sim 10^{-2}$ m tissues[5] can now be performed using commercial solutions, although most aspects continue to be designed in-house to suit particular biological sample handling requirements, such as the fixation to the force apparatus. Here we present a simple and inexpensive technique for applying known forces in the 10^{-6} to 10^{-3} N range on $\lesssim 10^{-2}$ m biological samples by using the attractive force between a permanent magnet and a millimetric steel sphere that is glued to the probed tissue. A typical setup using our force apparatus is shown in Fig. 1.

II. METHODS

We used high precision steel spheres (New England Miniature Ball Corp., Norfolk, CT) of 3 different radii— $r_b = 0.122$, 0.253, and 0.398 mm (± 0.01 mm, as measured on micrographs)—made of AISI 440 C martensitic ferromagnetic stainless steel (density $\rho_b = 7650$ kg/m^3). The permanent magnet is a commercial grade neodymium (Nd-Fe-B) axially magnetized disk (nickel plated, diameter $2a = 7.5$ mm and height $t = 2.8$ mm; The Magnet Source, Castle Rock, CO).

The interaction between the magnet and the bead was calibrated by immersing the steel ball in pure glycerol (den-

sity $\rho_f = 1261$ kg/m^3, viscosity $\eta_f = 0.690$ Pa s at 29 °C) at the tip of a conical support; the magnet was then brought above the bead (cylindrical edges facing the bead, flat edges oriented vertically), and the motion of the bead was simultaneously video-recorded at 250 frames per second (fps) using a digital camera (PL-B781, PixeLINK, Ottawa, ON) equipped with an objective that magnified to 45 μm/px1 (see movie S1 in the supplementary material).[6] All materials used to manipulate the bead and the magnet had no magnetic susceptibility. Movies were processed off-line using the IDL language (ITT Visual Information Solutions, Boulder, CO) in order to extract the position of the bead and of the magnet. We used a particle tracking package[7] to extract the bead trajectory, and the magnet was tracked using image registration of a reference sub-array in each frame: the reference image was manually clipped from the initial frame to contain the intensity pattern of the feature to be tracked, and was then aligned in the remaining frames onto the mobile matching pattern by maximizing intensity correlation.[8] These trajectory extraction methods offer a resolution that we estimated as being about 1/2 pixel, that is, ~ 20 μm.

The equation describing the motion of a sphere in a viscous fluid is[9]

$$\frac{4}{3}\pi r_b^3\left(\rho_b + \frac{\rho_f}{2}\right)\dot{v}(t) = F - 6\pi\eta_f r_b v(t) - \frac{4}{3}\pi r_b^3(\rho_b - \rho_f)g$$
$$- 6r_b^2(\pi\eta_f\rho_f)^{1/2}\int_0^t \frac{\dot{v}(\tau)d\tau}{(t-\tau)^{1/2}}, \tag{1}$$

in which the rate of change of the momentum of the sphere (left-hand side) is balanced by, in order of appearance on the right-hand side, the magnetic force F (to be determined), the drag force, the weight, and the Boussinesq-Basset force. Here, $v(t)$ and $\dot{v}(t)$ are, respectively, the velocity and the acceleration of the bead at time t, and $g = 9.81$ m/s^2 is gravity. In the regime of operation, we find that the Reynolds number $\rho_f r_b v/\eta_f < 10^{-1}$ at all times, so that the unsteady effects due to the Boussinesq-Basset force are negligible.

a)Currently at the Department of Materials, ETH Zürich, Switzerland.
b)Author to whom correspondence should be addressed. Electronic mail: lm@seas.harvard.edu.
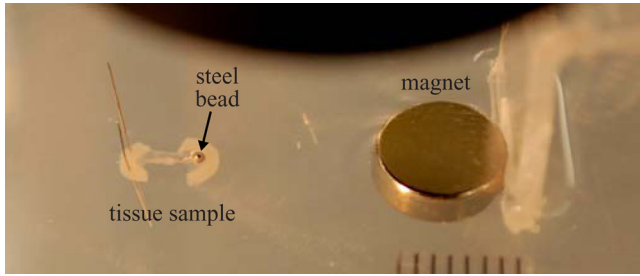
111, 074704-1

FIG. 1. View of the tensile test setup; the sample and the magnet sit on agarose, and both are immersed in buffer. The shaded area at the top of the figure is the microscope objective, and the ruler's divisions are in millimeters.

By tracking the bead as a function of the distance d between the center of the ball and the cylindrical edge of the magnet, as shown in Fig. 2, we find a set of reproducible curves $F(d)$, which are unchanged even when the steel balls are in contact with the magnet prior to the measurement. Over the range of distance of $2\,mm < d < 8\,mm$, the force follows a power-law scaling $F(d) = F_0\,(d_0/d)^\alpha$, in which F_0 is the characteristic magnitude of the force $F_0 = F(d = d_0)$ at the characteristic distance $d_0 = 1\,mm$. The table in Fig. 2 summarizes the power-law fitting parameters we measured for each ball radius. Although the magnetic force follows closely the simple law $F(d) \propto r_b^3 d^{-4}$ and is in good agreement with a theory for the interaction of magnetic point dipoles (see Appendix A), the approximation inherent in the scaling theory for the magnet breaks down when the distance between the magnet and the ball $d \leq 2\,a$. The point dipole approximation eventually gives way to a more detailed model that correctly interprets the curves of Fig. 2 by accounting for both the finite size of the magnet and the field-dependent magnetization of the steel ball (see Appendix A).

Together with this model, the force calibration allows us to extract the magnetic properties of the alloy; in particular, we find that the magnetic permeability of the material $\mu \approx 20$ and the coercive force $H_c \approx 5 \times 10^3$ A/m (see Appendix A). Steel 440 C has a high concentration of carbon (about 1% by
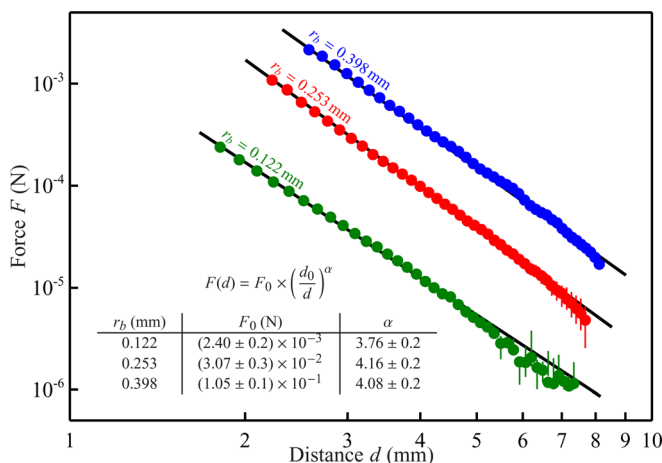
weight), which is known to enhance magnetic hardness (i.e., "low" $\mu < 100$ and "high" $H_c \approx 3 \times 10^3$ A/m, as obtained by extrapolating data from Refs. 10 and 11 for very similar materials), consistent with our findings. Furthermore, we note that because the coercive force is reached when the distance $d = 8$ mm, any remanent magnetization of the ball has no consequence on the calibration curves for $d \leq 8$ mm.

III. APPLICATIONS

In order to show how the method can be deployed at the mesoscale, we used this simple force apparatus to perform tensile tests on two archetypal embryonic tissue types that highlight the linear and nonlinear elasticity of these soft materials. We chose to work on the vertebrate gut early in its developmental history, when it is a relatively simple homogeneous tube of undifferentiated tissue that is attached to the body via a thin mesentery tissue.[12] As this tissue has been used in case studies for mechanical measurements in the past[5,13] and the stiffnesses of these components are directly implicated in directing the final morphogenetic patterns of the organ,[12] our study serves as a careful evaluation of the method while producing results that are directly relevant for a biological problem.

A. Tissue manipulation

All dissections and further tissue manipulations were performed in Ringer buffer (Sigma Aldrich, St. Louis, MO) under a binocular microscope. The millimetric beads were handled using forceps (or an aspiration micropipette for the smaller ones). We used various methods to attach the bead to one extremity of the tissue sample, depending on its shape, and we give two examples in Secs. III B and III C. The sample was then laid out on agarose molded in a Petri dish, and its other end was pinned on the gel substrate. The magnet, attached to a plastic arm held on a micrometric translation stage, was brought toward the sample along its principal axis, as shown in Fig. 1. The magnet attracted the bead and stretched the sample in a controlled fashion. The magnet was moved toward the sample in a stepwise motion. At each step after the sample was extended, the next step was applied only after the sample was at mechanical equilibrium, as visually checked (see movie S2 in the supplementary material).[6] We thus ensured that the strain rate was less than 10^{-3} s^{-1}, so that we were effectively probing only the static elasticity of the tissue.[5,14] Because the thickness of the tissue is small, our method ensures that the applied force is uniform in the sample transverse section while avoiding the significant complications of other fixation techniques required for bulkier tissue samples.[15] The tensile tests were video-recorded under a binocular microscope (2 fps with a magnification $\sim 10\,\mu m$/pxl) in order to track the extension L of the sample and the distance from bead to magnet d with a 5 μm resolution (which translates to a 1% error on the force determination), by using the same methods as described above (see the "Methods" section). Figs. 3(a) and 4(a) show examples of the trajectories of the bead and the magnet. All measurements were carried out within a few hours after dissection.

$$F(d) = F_0 \times \left(\frac{d_0}{d}\right)^\alpha$$

| r_b (mm)	F_0 (N)	α
0.122	$(2.40 \pm 0.2) \times 10^{-3}$	3.76 ± 0.2
0.253	$(3.07 \pm 0.3) \times 10^{-2}$	4.16 ± 0.2
0.398	$(1.05 \pm 0.1) \times 10^{-1}$	4.08 ± 0.2

FIG. 2. Force vs distance calibration curves for 3 different sizes of steel ball; the black lines are the power-law fit, the parameters of which are presented in the inset ($d_0 = 1$ mm).
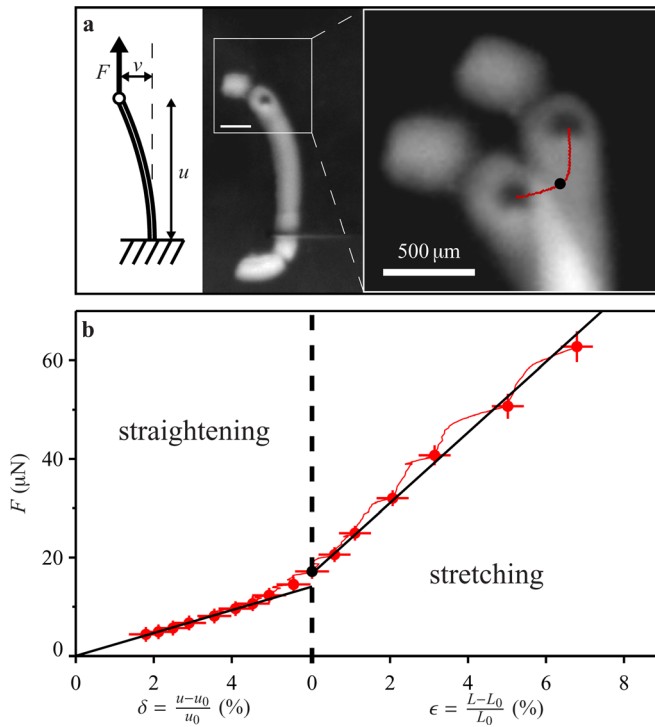
FIG. 3. (a) The curved tube tissue sample at rest. The $3\times$ magnification shows the trajectory followed by the ball (red) as the magnet approaches (from the top) and applies an axial load, overlaid on the first and last movie frame; the point separates the straightening and the stretching regime. (b) The corresponding force vs extension curve in the two regimes (we use a different definition of the strain in each regime).

B. Tubular tissue

In the first illustrative experiment, we mechanically tested cylindrical tissue, the gut tube, extracted from chicken intestine at embryonic day 12. The steel bead was
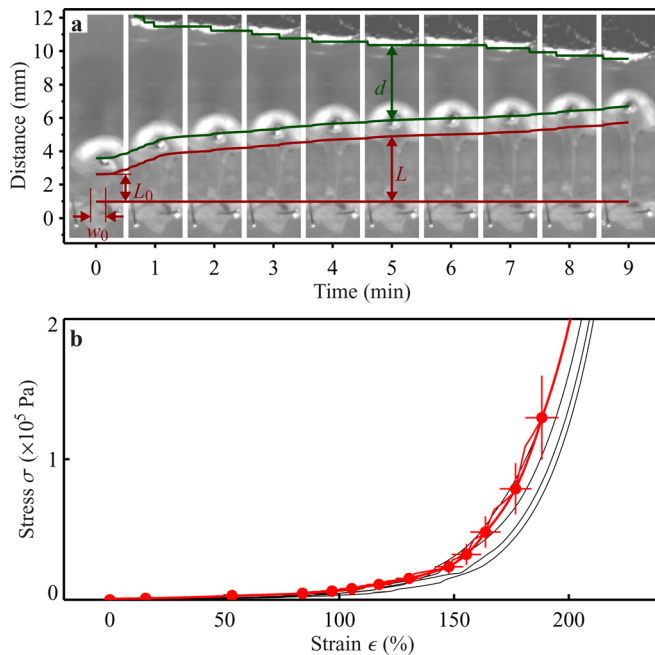

FIG. 4. (a) The stepwise approach of the magnet stretches the sample by an amount L/L_0 that can be tracked as a function of the bead-to-magnet distance d. (b) The resulting stress vs strain mechanical response of the mesentery sample (red), reproduced for several other samples (black).

inserted inside the tube and secured by means of closing the lumen using a hair with an overhand knot. The other end of the tube was held on the agarose gel with a horseshoe pin [see Fig. 3(a)]. We then brought the magnet toward the gut while measuring the weak deformations of the tube. Because the tube sample has a slight curvature, we used the force apparatus to measure the axial load required in order to first straighten the tube and then stretch the tube to a small strain. These two regimes provide two independent ways to measure the Young's modulus E of the material of the tube. In the first regime, using the notation of Fig. 3(a), the torque due to the force is given by Fv, and the resisting bending moment is $2EI[(v/u^2) - (v_0/u_0^2)]$, in which (u_0, v_0) is the configuration of the curved tube at rest ($v_0 \ll u_0$) and $I = (\pi/4)(r_o^4 - r_i^4)$ is the axial area moment of inertia for a tube with inner and outer radii $r_i = 72 \pm 9\,\mu m$ and $r_o = 209 \pm 12\,\mu m$, respectively (see Appendix B). If we let $\delta = (u - u_0)/u_0 \ll 1$ be the relative displacement and $L_0 \approx (u^2 + v^2)^{1/2}$ be the tube length (assumed invariant in the straightening regime), the moment balance then gives $F \approx 2(EI/v_0^2)\delta$; the exact result $F = \frac{15}{8}(EI/v_0^2)\delta$ for a beam *uniformly curved* at rest is derived in Ref. 16. In the second regime, once the tube is straight, the tensile force $F = EA_0\epsilon$ [with $A_0 = \pi(r_o^2 - r_i^2)$] acting on the tube section yields a strain $\epsilon = (L - L_0)/L_0$ at the tracked location L. In Fig. 3(b) we do indeed observe two regimes for the force-extension response of the curved tube; during straightening, starting from a deflexion $v_0/r_0 = 1.3 \pm 0.1$ [see Fig. 3(a)], we measure $dF/d\delta = 230 \pm 30\,\mu N$, and during stretching, $dF/d\epsilon = 715 \pm 30\,\mu N$. This gives the two independent estimates of the Young's modulus $E = 5.8 \pm 1.5\,kPa$ and $E = 5.9 \pm 0.8\,kPa$ in the straightening and stretching regimes, respectively (the tube shape introduces a bias of at most 20% in the extraction of E with low-strain tensile tests[17]) and effectively confirms that the tube material can be considered homogeneous on length scales $\sim r_o$.

C. Membranous tissue

In the second illustrative experiment, we focused on the nonlinear force-extension curve for a very soft tissue, the mesentery, a thin sheet that attaches the gut to the rest of the body. Performing similar low strain tensile tests on the mesentery involves forces of $0.1\,\mu N$ that are outside of the range that is accessible with our technique. This limitation precludes probing the linear response of such soft tissue of this size with our technique. Nevertheless, our method allows us to probe the finite deformation response of such tissues. We surgically dissected fragments of the mesentery from live chickens at embryonic day 16. The samples were carefully cut out so as to leave a well-defined constant millimetric width strip, on one end of which the steel bead was glued using synthetic glue (Instant Krazy Glue, Columbus, OH). Upon contact with the medium, the glue hardens to permanently seal the bead to the membrane, leaving the surrounding tissue unaffected. For more delicate samples, a biomolecular coating could be used to attach the bead to the tissue. The other end of the tissue strip was pinned to the agarose gel layer [Figs. 1 and 4(a)]. During dissection, we

usually kept sections of the tube or of the superior mesenteric artery, as they provided convenient handles with which to manipulate or pin the fragments and to glue the bead (see Figs. 1 and 4(a), in which sections of the tube are clearly visible). For large deformation assays, the sample was first preconditioned by stretching it once to an extension ratio greater than 1, after which the magnet was removed so as to let the sample relax to its rest length L_0 (movie S2),[6] at which stage we visually extracted the rest width w_0 of the mesentery strip. This pre-conditioning stage, shown in the first 10 min of movie S2,[6] is commonly employed to produce reliable large deformation mechanical measurements that are relatively independent of previous manipulations.[5,14,18] The magnet was then moved back toward the sample in a step-wise motion. Using the cross-section area of the sample at rest $A_0 = w_0 h_0$, with $h_0 = 12.7 \pm 2.8\ \mu m$ being the thickness of the unstretched mesentery (see Appendix B), allows us to plot the nominal stress $\sigma = F(d)/A_0$, calculated from the known force, against the nominal strain $\epsilon = (L - L_0)/L_0$ in order to quantify the mechanical response of the material for $\epsilon \lesssim \epsilon_p = 218\% \pm 15\%$, the physiological strain (see Appendix B and Ref. 12). More sophisticated methods for extracting the local strain field could be used in that case (for example, tracking small features in the sample strip). However, we infer that the nominal strain is sufficient for evaluating the non-linear mechanical response of the mesentery material at the large strain found in physiological conditions. Several stress-strain response curves, corresponding to samples of mesentery extracted from different day 16 chicken embryos, are shown in Fig. 4(b) and verify that our method returns reproducible results, with same-sample variations that are below the sample-to-sample variations, measured at about 50% [Fig. 4(b)]. Notably, we observe the typical strain-stiffening around $\epsilon \approx \epsilon_p$ of biological soft tissues.[18]

IV. CONCLUSION

These two tests serve to show that our method will be of practical value for a wide variety of mechanical tests on various types of tissue. Possible extensions of the method include the use of an oscillatory force (e.g., with an electromagnet), although in that case the dynamic response of the bead in the fluid would need to be carefully scrutinized as well.

APPENDIX A: MODEL OF THE INTERACTION BETWEEN THE BEAD AND THE MAGNET

The magnetic field strength $\mathbf{H}^0(\mathbf{r})$ generated at a position $\mathbf{r}$ from the center of an axially magnetized disk magnet with a radius a and height t can be computed exactly. In the (r,z) cylindrical coordinates basis, in which z is on the cylinder's axis and $z = 0$ at its center, and where $\mathbf{M}^0 = (0, M^0)$ is its uniform magnetization, $\mathbf{H}^0(\mathbf{r}) = (H_r^0, H_z^0)$ is given by[19]

$$H_{r/z}^0 = \frac{M^0}{2}\left[f_{r/z}\left(r, z - \frac{t}{2}\right) - f_{r/z}\left(r, z + \frac{t}{2}\right)\right] \quad \text{(A1)}$$

with

$$f_r(r,z) = \int_0^\infty J_1(ua)J_1(ur)e^{-uz}a\,du, \quad \text{(A2a)}$$

$$f_z(r,z) = \int_0^\infty J_1(ua)J_0(ur)e^{-uz}a\,du \quad \text{(A2b)}$$

for $\mathbf{r}$ external to the magnet. Here J_n is the nth-order Bessel function of the first kind. One can express the functions $f_{r/z}(r,z)$ in term of the complete elliptic integrals of the first, second, and third kind, $K(k)$, $E(k)$, and $\Pi(p|k)$, respectively, defined as

$$K(k) = \int_0^{\pi/2}(1 - k^2\sin^2\theta)^{-1/2}d\theta, \quad \text{(A3a)}$$

$$E(k) = \int_0^{\pi/2}(1 - k^2\sin^2\theta)^{1/2}d\theta, \quad \text{(A3b)}$$

$$\Pi(p|k) = \int_0^{\pi/2}(1 - p\sin^2\theta)^{-1}(1 - k^2\sin^2\theta)^{-1/2}d\theta. \quad \text{(A3c)}$$

Calling the elliptic modulus $k^2 = 4ar/[(a + r)^2 + z^2]$ and the elliptic characteristic $p = 4ar/(a + r)^2$, we get[20]

$$f_r(r,z) = \frac{2a}{k\pi\sqrt{ar}}\left[\left(1 - \frac{1}{2}k^2\right)K(k) - E(k)\right] \quad \text{(A4)}$$

and

$$f_z(r,z) = \frac{kz}{2\pi\sqrt{ar}}\left[\left(\frac{r - a}{r + a}\right)\Pi(p|k) - K(k)\right] + \begin{cases} 1 & \text{if } r < a, \\ 0 & \text{if } r \geq a. \end{cases} \quad \text{(A5)}$$

In Fig. 5(a) we show the density map and stream lines of the field $\mathbf{H}^0$ generated from the magnet, as calculated using the formula above. In Fig. 5(b), we quantitatively compare this model with experimental measurements of $H_z^0(r = d + a, 0)$ and $H_z^0(0, z = d + t/2)$ obtained with a Gaussmeter probe (F.W. Bell/Sypris Solution, Inc.). To produce Figs. 5(a) and 5(b), we have used $M^0 = 9.7 \times 10^5$ A/m for Nd-Fe-B materials,[19] and the dimensions of the magnet are $a = 3.75$ mm and $t = 2.80$ mm. Notably, $H_z^0(d + a, 0)$ in the range $d \leq 2a$ does not follow the d^{-3} scaling that would be obtained for the field generated by a magnetic point dipole. We verify, however, the correct limits $\mathbf{H}^0(\mathbf{r}) = 1/(4\pi|\mathbf{r}|^5)[3\mathbf{r}(\mathbf{m}^0 \cdot \mathbf{r}) - \mathbf{m}^0(\mathbf{r} \cdot \mathbf{r})]$ with $\mathbf{m}^0 = (\pi a^2 t)\mathbf{M}^0$ for $|\mathbf{r}| \gg a$, which is the field generated from a point dipole $\mathbf{m}^0$.

We then proceed by using Kelvin's expression of the force on a sphere,[21] $\mathbf{F} = -\mu_f \frac{4}{3}\pi r_b^3\ \mathbf{M} \cdot (\nabla\mathbf{H}^0)$, in which $\mu_f \approx \mu_0 = 4\pi \times 10^{-7}$ N/A^2 is the fluid magnetic permeability and $\mathbf{M}$ is the magnetization of the ferromagnetic sphere, assumed to be uniform in the bead's volume but dependent on $\mathbf{H}^0$. The trajectory of the ball indicates that $\mathbf{F} = (-F, 0)$, with $F = \mu_0\frac{4}{3}\pi r_b^3 M(dH_z^0/dr)|_{\mathbf{r}=(r,0)}$; we have used $\mathbf{M} \cdot (\nabla\mathbf{H}^0) = \mathbf{M} \cdot (\nabla\mathbf{H}^0)^T$ because $\mathbf{H}^0$ is irrotational. We find
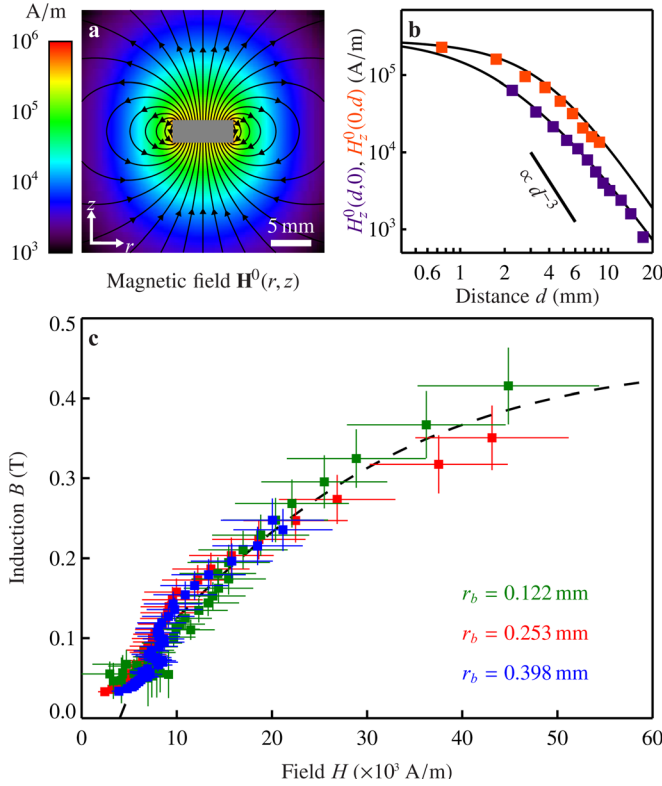
FIG. 5. (a) Map and streamlines of the magnetic field $\mathbf{H}^0$ generated by the magnet. (b) Measurements of the axial field H_z^0 at $r = 0$ and at $z = 0$. (c) Magnetization curve of the steel 440 C, inferred from the force curves.

$$\frac{dH_z^0}{dr}\bigg|_{\mathbf{r}=(r,0)} = \frac{dH_r^0}{dz}\bigg|_{\mathbf{r}=(r,0)} = \frac{M^0}{2}\frac{kt}{2\pi r\sqrt{ar}}$$
$$\times \left[\left(\frac{2-k^2}{2-2k^2}\right)E(k) - K(k)\right], \qquad \text{(A6)}$$

with $k^2 = 4ar/[(a+r)^2 + (t/2)^2]$. If one assumes that the magnetization of the ball is saturated at all positions relative to the magnet, one finds $F(d) \sim \mu_0(mm^0/d^4)$ from Kelvin's formula in the limit $d = |\mathbf{r}| - a \gg a$ (point dipole limit), with $m^0 = \pi a^2 t M^0$ and $m = \frac{4}{3}\pi r_b^3 M$. As stated in the main text, this approximation is not valid here, even if the measured scaling for $F(d)$ appears to agree.

From the force calibration curve F (Fig. 2) and the known field H_z^0 at $z = 0$ [Fig. 5(b)], we can calculate M as a function of H^0 using Kelvin's formula. We present our result in Fig. 5(c) in the more standard "B versus H" form; the internal fields are $H = H_z^0 - \frac{1}{3}M$ and $B = \mu_0(H + M)$, as calculated for a permeable sphere.[19] The ball size r_b^3-dependence of the force is outlined in the main text; thus the (H, B) data obtained for the three different beads all fall on the same curve that characterizes the magnetic response of their AISI 440 C stainless steel material. From this curve we can evaluate the maximum magnetic permeability $\mu = \max(B/\mu_0 H) \approx 20$, the coercive force $H_c \approx 5 \times 10^3$ A/m such that $B(H_c) = 0$, and the remanent flux $B_r \approx 0.5$ T by extrapolation. These magnetic properties are in close agreement with tabulated data for similar ferromagnetic steel alloys,[10,11] as explained in the main text.
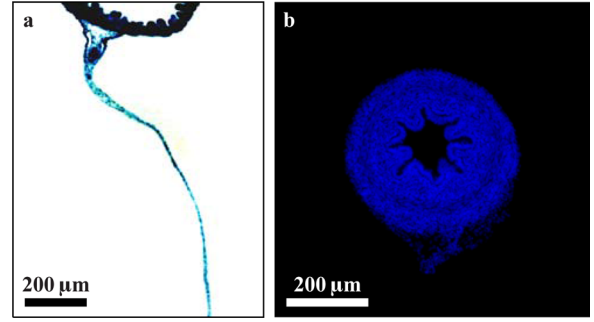

FIG. 6. (a) Cross section of the mesentery at embryonic day 16. The gut tube can be seen at the top of the image. (b) Cross section of the gut tube at embryonic day 12. The connection to the mesentery is visible at the "6 o'clock" orientation.

APPENDIX B: CROSS SECTION MEASUREMENTS

Small intestines were collected from chicken embryos at day 16 and were fixed in 4% paraformaldehyde in phosphate-buffered saline, dehydrated in a graded ethanol series, cleared in xylenes, and embedded in paraffin. This allowed transverse sections 10 μm in thickness to be created and collected on glass slides. Fast Green staining was performed using standard protocols;[22] briefly, slides were dewaxed in xylenes, rinsed in successive washes with 100% and 95% ethanol, and rehydrated in tap water. Slides were then stained with Fast Green (Sigma Aldrich, St. Louis, MO) for 30 min, rinsed in tap water, dehydrated, cleared in xylenes, and mounted with DPX (Fluka-Sigma Aldrich, St. Louis, MO). A micrograph showing one of these sections is presented in Fig. 6(a). Such micrographs were used to measure the mesentery thickness $h = 7.1 \pm 1.4$ μm under physiological conditions, in which the mesentery is under tension. The physiological strain ϵ_p of the mesentery is found by measuring the deformed and rest lengths of strips L_p and L_0, respectively, before and after surgical isolation from the intestine. We find $\epsilon_p = (L_p - L_0)/L_0 = 218\% \pm 15\%$, a typically large value for this organ that is also encountered in other species.[5,13] Assuming material incompressibility, we find the rest thickness of the mesentery $h_0 = (1 + \epsilon_p)^{1/2}h = 12.7 \pm 2.8$ μm. We use this value in the main text to calculate the cross-section rest area of the sample of mesentery tissue.

DAPI (Molecular Probes, Invitrogen, Carlsbad, CA) was used as a nuclear stain on sections of the tube obtained in a similar way for embryos at day 12, in order to determine the size of the inner and outer radii (r_i and r_o, respectively) of the gut tube from the fluorescent micrographs shown in Fig. 6(b). We found $r_i = 72 \pm 9$ μm and $r_o = 209 \pm 12$ μm after averaging over 10 sections extracted from different locations along the tube.

[1]D. S. Gianola and C. Eberl, JOM **61**, 24 (2009).
[2]M. Dao, C. T. Lim, and S. Suresh, J. Mech. Phys. Solids **51**, 2259 (2003).
[3]C. Wiebe and G. W. Brodland, J. Biomech. **38**, 2087 (2005).
[4]L. A. Davidson and R. Keller, in *Cell Mechanics, Methods in Cell Biology*, Vol. 83 (Elsevier, 2007), pp. 425–439.
[5]Y. C. Fung, Am. J. Physiol. **213**, 1532 (1967). Available at http://ajplegacy. physiology.org/content/213/6/1532.
[6]See supplementary material at http://dx.doi.org/10.1063/1.3699176 for movies S1 and S2 and their legends.

[7]J. C. Crocker and D. G. Grier, J. Colloid Interface Sci. **179**, 298 (1996).

[8]H. Xie, N. Hicks, G. R. Keller, H. Huang, and V. Kreinovich, Comput. Geosci. **29**, 1045 (2003).

[9]L. D. Landau and E. M. Lifshitz, *Fluid Mechanics*, 2nd ed. (Pergamon, Oxford, England, 1987).

[10]R. M. Bozorth, *Ferromagnetism* (Van Nostrand, New York, 1951).

[11]P. Oxley, J. Goodell, and R. Molt, J. Magn. Magn. Mater. **321**, 2107 (2009).

[12]T. Savin, N. A. Kurpios, A. E. Shyer, P. Florescu, H. Liang, L. Mahadevan, and C. J. Tabin, Nature **476**, 57 (2011).

[13]J. Hildebrandt, H. Fukaya, and C. J. Martin, J. Appl. Physiol. **27**, 758 (1969). Available at http://jap.physiology.org/content/27/5/758.

[14]R. M. Kenedi, T. Gibson, J. H. Evans, and J. C. Barbenel, Phys. Med. Biol. **20**, 699 (1975).

[15]J. Lepetit, R. Favier, A. Grajales, and P. O. Skjervold, J. Biomech. **37**, 557 (2004).

[16]C. González and J. LLorca, Int. J. Solids Struct. **42**, 1537 (2005).

[17]R. Mahmoodian and K. Van Vliet, private communication (June 2011).

[18]Y. C. Fung, *Biomechanics: Mechanical Properties of Living Tissues*, 2nd ed. (Springer-Verlag, New York, 1993).

[19]D. J. Craik, *Magnetism: Principles and Applications* (Wiley, New York, 1995).

[20]G. Eason, B. Noble, and I. N. Sneddon, Philos. Trans. R. Soc. London **247**, 529 (1955).

[21]A. Engel and R. Friedrichs, Am. J. Phys. **70**, 428 (2002).

[22]N. A. Kurpios, M. Ibañes, N. M. Davis, W. Lui, T. Katz, J. F. Martin, J. C. I. Belmonte, and C. J. Tabin, Proc. Natl. Acad. Sci. U.S.A. **105**, 8499 (2008).